Malonate-based inhibitors of mammalian serine racemase: Kinetic characterization and structure-based computational study

ARTICLE *in* EUROPEAN JOURNAL OF MEDICINAL CHEMISTRY · JANUARY 2015

Impact Factor: 3.45 · DOI: 10.1016/j.ejmech.2014.10.043

11 AUTHORS, INCLUDING:

Dana Nachtigallová
Academy of Sciences of the Czech Republic
71 PUBLICATIONS **1,824** CITATIONS
SEE PROFILE

Michal Otyepka
Palacký University of Olomouc
181 PUBLICATIONS **4,521** CITATIONS
SEE PROFILE

Pavel Hobza
Academy of Sciences of the Czech Republic
317 PUBLICATIONS **18,095** CITATIONS
SEE PROFILE

Martin Lepsík
Academy of Sciences of the Czech Republic
52 PUBLICATIONS **696** CITATIONS
SEE PROFILE

European Journal of Medicinal Chemistry 89 (2015) 189–197

Contents lists available at ScienceDirect

European Journal of Medicinal Chemistry

journal homepage: http://www.elsevier.com/locate/ejmech

Original article

Malonate-based inhibitors of mammalian serine racemase: Kinetic characterization and structure-based computational study

Barbora Vorlová [a, b, 1], Dana Nachtigallová [a, 1], Jana Jirásková-Vaníčková [a, b], Haresh Ajani [a, c], Petr Jansa [a], Jan Řezáč [a], Jindřich Fanfrlík [a], Michal Otyepka [c], Pavel Hobza [a, c], Jan Konvalinka [a, b, *], Martin Lepšík [a, **]

[a] Institute of Organic Chemistry and Biochemistry, Gilead Sciences and IOCB Research Centre, Academy of Sciences of the Czech Republic, v.v.i., Flemingovo nam. 2, 166 10 Prague 6, Czech Republic
[b] Department of Biochemistry, Faculty of Natural Science, Charles University, Albertov 6, 128 43 Prague 2, Czech Republic
[c] Regional Centre of Advanced Technologies and Materials, Department of Physical Chemistry, Palacky University, 771 46 Olomouc, Czech Republic

ARTICLE INFO

Article history:
Received 19 May 2014
Received in revised form
14 October 2014
Accepted 14 October 2014
Available online 16 October 2014

Keywords:
NMDA receptor
Pyridoxal-5′-phosphate-dependent enzyme
Human/mouse serine racemase
Malonate-based inhibitors
Semiempirical quantum mechanical calculations
Docking
Water thermodynamics

ABSTRACT

Overactivation of NMDA receptors has been implicated in various neuropathological conditions, including brain ischaemia, neurodegenerative disorders and epilepsy. Production of D-serine, an NMDA receptor co-agonist, from L-serine is catalyzed *in vivo* by the pyridoxal-5′-phosphate (PLP)-dependent enzyme serine racemase. Specific inhibition of this enzyme has been proposed as a promising strategy for treatment of neurological conditions caused by NMDA receptor dysfunction.

Here we present the synthesis and activity analysis of a series of malonate-based inhibitors of mouse serine racemase (mSR). The compounds possessed IC_{50} values ranging from 40 ± 11 mM for 2,2-bis(hydroxymethyl)malonate down to 57 ± 1 μM for 2,2-dichloromalonate, the most effective competitive mSR inhibitor known to date. The structure–activity relationship of the whole series in the human orthologue (hSR) was interpreted using Glide docking, WaterMap analysis of hydration and quantum mechanical calculations based on the X-ray structure of the hSR/malonate complex. Docking into the hSR active site with three thermodynamically favourable water molecules was able to discern qualitatively between good and weak inhibitors. Further improvement in ranking was obtained using advanced PM6-D3H4X/COSMO semiempirical quantum mechanics-based scoring which distinguished between the compounds with IC_{50} better/worse than 2 mM. We have thus not only found a new potent hSR inhibitor but also worked out a computer-assisted protocol to rationalize the binding affinity which will thus aid in search for more effective SR inhibitors. Novel, potent hSR inhibitors may represent interesting research tools as well as drug candidates for treatment of diseases associated with NMDA receptor overactivation.

1. Introduction

Neurotransmission in the mammalian brain is mediated by several receptors, including *N*-methyl-D-aspartate receptors (NMDARs). Overactivation of these glutamate receptors has been implicated in neuropathological conditions such as brain ischaemia, neurodegenerative disorders and epilepsy [1]. For treatment of these diseases, high-affinity NMDAR blockers are used. However, most of these drugs have undesirable side effects, and therefore, new strategies to regulate NMDAR activity are needed.

To fully activate NMDARs, two different binding sites—the glutamate (agonist) site and the so-called “glycine” (co-agonist) site—need to be occupied [2]. While only glutamate can bind to the agonist site, the co-agonist site can be occupied by either glycine or

Abbreviations: MD, molecular dynamics; NMDAR, *N*-methyl-D-aspartate receptor; PLP, pyridoxal-5′-phosphate; SR (hSR, mSR), serine racemase (human, mouse); QM, quantum-mechanical; PM6-D3H4X, PM6, parametrized model 6 semiempirical quantum mechanical method; D3, 3rd generation dispersion correction; H4, 4th generation hydrogen-bonding correction; X, halogen bonding correction; COSMO, conductor-like screening model of implicit solvent; SMD, solvation model based on density; HF, Hartree–Fock; SQM, semiempirical quantum-mechanical; ADP, atomic displacement parameter; CCSD(T)/CBS, coupled-cluster singles doubles and iterative triples at complete-basis-set limit.

* Corresponding author. Institute of Organic Chemistry and Biochemistry, Gilead Sciences and IOCB Research Centre, Academy of Sciences of the Czech Republic, v.v.i., Flemingovo nam. 2, 166 10 Prague 6, Czech Republic.
** Corresponding author. Institute of Organic Chemistry and Biochemistry, Gilead Sciences and IOCB Research Centre, Academy of Sciences of the Czech Republic, v.v.i., Flemingovo nam. 2, 166 10 Prague 6, Czech Republic.
E-mail addresses: konval@uochb.cas.cz (J. Konvalinka), lepsik@uochb.cas.cz (M. Lepšík).
[1] Both authors contributed equally to this work.

http://dx.doi.org/10.1016/j.ejmech.2014.10.043
0223-5234/

D-serine. Based on early experiments, it was proposed that either of these compounds could serve as the main NMDAR co-activator, depending on the brain region [3]. However, more recent reports prioritize D-serine, rather than glycine, as the major NMDAR co-agonist [4]. In this context, specific inhibition of the main enzyme responsible for synthesis of D-serine — serine racemase (SR) — may be a promising strategy for regulation of NMDAR overstimulation [5–7].

Serine racemase is a pyridoxal-5′-phosphate (PLP) dependent enzyme that produces D-serine from L-serine [8]. Its activity increases in the presence of divalent cations (Mg^{2+}, Mn^{2+} or Ca^{2+}) [9,10] and several nucleotides (of which ATP is the most effective activator) [11,12]. The best studied mammalian serine racemases — rat, mouse and human — share approximately 90% sequence homology. The residues responsible for the binding of PLP and activators (ATP and divalent cations) are highly conserved among these SR orthologues [13].

Three-dimensional structures obtained from X-ray crystallographic analysis are available for rat SR (PDB codes 3L6C and 3HMK) and human SR (PDB codes 3L6R and 3L6B) [14]. hSR consists of two domains that form the active site. The enzyme can adopt two different conformations: the open conformation, in which the active site is empty, and the closed conformation, in which the active site is occupied by either a substrate or competitive inhibitor [15]. The existence of two distinct conformations of SR has been recently confirmed by ATP-binding studies. Indeed, it was shown that ATP binding to the ligand-free and ligand-occupied forms exhibits striking differences [16].

To date, efforts to find potent mammalian SR inhibitors have not been very successful; the most effective compounds—malonate and L-*erythro*-3-hydroxyaspartate—exhibit rather weak binding constants in the micromolar range [17,18]. Several different strategies have been employed in the search for a potent SR inhibitor (for review, see Ref. [13]). Most studies have focused on systematic modification of L-serine and L-serine-*O*-sulphate [9,17]. Screenings of a wide panel of amino acids [12,19], small peptides [20] and other miscellaneous compounds structurally unrelated to serine [13,18] have also been performed with little success.

Attempts have been made to rationalize the activity of dicarboxylate mSR inhibitors by applying quantum chemical (QM) calculations to the ligands. These studies revealed that the optimal length of a linker between the carboxylate moieties is two to three methylene groups [17]. The long-strived-for elucidation of mammalian SR 3D structures [14] has opened the possibility of rational structure-based design of potent hSR inhibitors. Recently, Mori and co-workers identified novel SR inhibitors using *in silico* screenings and subsequent evaluation of 'hit molecules' by *in vitro* enzyme assay. Two of the reported inhibitors possessed lower IC_{50} value than malonate [21].

The X-ray structure of the hSR/malonate inhibitor complex shows a highly polar active site lined with charged and polar residues and PLP cofactor. The active site is filled with structural water molecules even in the presence of this dianionic inhibitor. Both these facts present a challenge for computational drug design, due to the need of accurate treatment of electrostatics as well as water dynamics and thermodynamics.

Positions of structural water molecules and their enthalpy and entropy contributions can be predicted via methods such as GRID [22], HINT/Rank [23], JAWS [24] or WaterMap [25] algorithms. Such approaches proved crucial in rationalizing the ligand binding affinity to factor Xa serine protease [25] or location of protein hydration sites [24].

Computational structure-based drug design has recently been enhanced with quantum-mechanical (QM) treatment of protein–ligand interactions, which allows description of quantum effects such as electron or proton transfer (reviewed in Refs. [26–28]) These techniques are advantageous when working with non-standard moieties such as metal ions [29] or inorganic ligands [30–32] or processes such as halogen bonding [33,34], proton transfer [35], charge redistribution or covalent binding [36].

In this work, we provide kinetic characterization of mouse SR (mSR) in the presence of a series of malonate-based inhibitors and evaluate their inhibitory potency. We analyze the compounds using docking, analysis of hydration and semiempirical QM calculations. The computational analyses reveal the profound effects of the thermodynamically-favourable active-site water molecules on the compound binding modes and show that SQM scoring can distinguish between good and weak binders. The suggested protocol can thus help guide future efforts in computer-aided drug design of hSR inhibitors.

2. Results

2.1. Inhibition of mouse serine racemase by malonate-based compounds

We prepared recombinant mSR using an *Escherichia coli* expression system and four-step purification, yielding 3.5 mg of purified mSR per 1 l culture. The mSR preparation was enzymatically active and capable of racemising and eliminating L-serine (K_M for L-serine racemisation = 3.4 ± 0.3 mM, V_{max} = 11.0 ± 0.3 μM/min).

We selected a panel of small, negatively charged molecules related to malonate and tested them for their potential to competitively inhibit serine racemisation by mSR. In the initial screening, a single concentration (5 mM ligand) was used to test the inhibitory activity (see Fig. 1).

The inhibitory potencies of the compounds that blocked the racemisation activity of mSR by more than 98% in these conditions (malonate, 2-hydroxymalonate, 2-aminomalonate and 2,2-dichloromalonate) were further kinetically characterized (see Table 1). Additionally, the half maximal inhibitory concentration (IC_{50}) of several less-active compounds was also determined (see Table 1). The IC_{50} values ranged from 57 ± 1 μM to 40 ± 11 mM.

2.2. Mechanism of inhibition

We determined the mechanism of action for the most active compounds (malonate and 2,2-dichloromalonate). Double reciprocal Lineweaver–Burk plots (see Fig. 2) of the kinetic data indicate that both compounds are competitive mSR inhibitors. The inhibition constant (K_i) for malonate was 27 ± 3 μM, while 2,2-dichloromalonate was a slightly more potent inhibitor, with a K_i value of 19 ± 3 μM.

2.3. hSR/malonate X-ray structure

2.3.1. Hydrogen bonding and active-site waters

Visual inspection of the hSR/malonate X-ray structure (PDB code: 3L6B) [14] revealed that the inhibitor is held in the hSR active site by numerous hydrogen bonds to both the protein backbone (Ser84:N, Asn86:N, His87:N) and amino acid side chains (Ser83:OG, Ser84:OG, Arg135:NH1, Arg135:NH2, Ser242:OG) (Fig. 3, Table 2). Additional protein–ligand hydrogen bonds are mediated by structural water molecules (W351, W372, W373, W403 and W436) (Fig. 3, Table 2).

Careful inspection of the active-site water molecules in this crystal structure showed close contacts between the oxygen of W351 and the oxygen of W436 (2.27 Å) and OG of Ser242 (2.50 Å), which would result in strong repulsion. Moreover, the W351

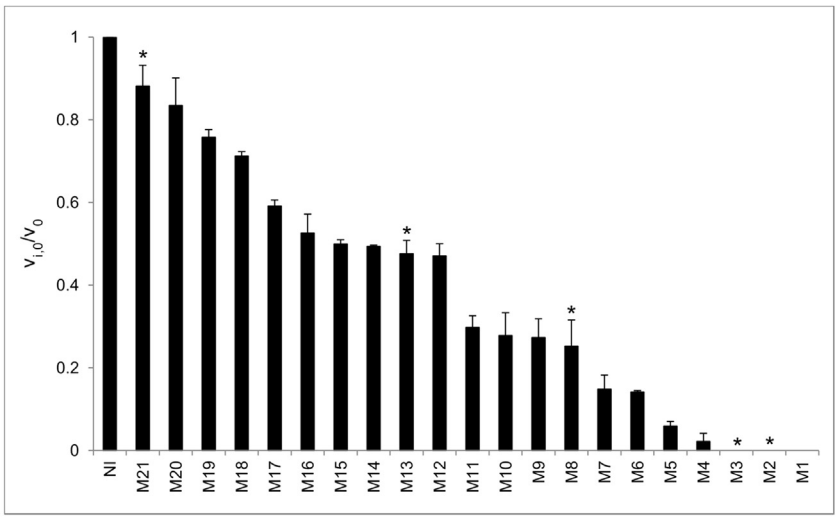

CODE	STRUCTURE	CODE	STRUCTURE	CODE	STRUCTURE
M1	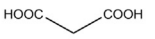	M8*	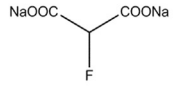	M15	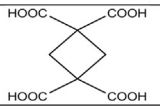
M2*	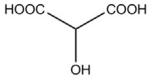	M9		M16	
M3*	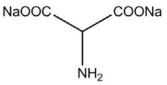	M10	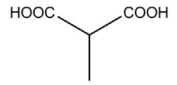	M17	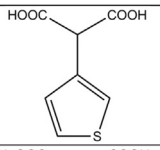
M4	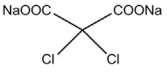	M11	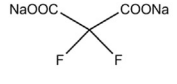	M18	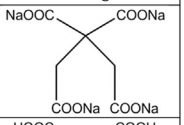
M5	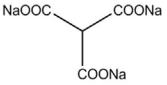	M12	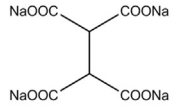	M19	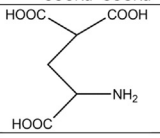
M6	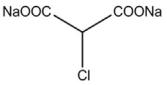	M13*	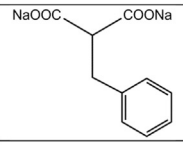	M20	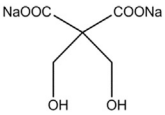
M7	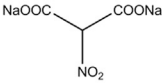	M14	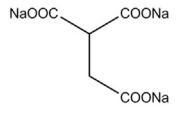	M21*	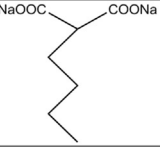

Fig. 1. Inhibition of mSR racemisation reaction by malonate-based compounds. Activity reactions were carried out at 37 °C in a pH 8.0 buffer containing 100 mM HEPES–NaOH, 10 μM pyridoxal-5′-phosphate, 1 mM $MgCl_2$, 5 mM DL-dithiothreitol, 1 mM ATP, 135 nM mSR, 5 mM L-serine and 5 mM test compound. Approximate results for compounds marked with an asterisk have been previously published by our group [13].

oxygen had approximately twice higher atomic displacement parameter (ADP, formerly B-factor) than the other structural water molecules (23 $Å^2$ for the former as opposed to an average of 12 $Å^2$ for the latter). This hinted at a possible refinement problem, which does not influence the overall model statistics but results in an unphysical structure that cannot be used for further computations.

To examine the water network surrounding malonate in a more rigorous way we used WaterMap program [38].

2.3.2. *WaterMap analysis of hSR/malonate X-ray structure*

The crystal structure of hSR/malonate complex including crystal water molecules was examined using WaterMap. The procedure identified six water molecules within 4.4 Å of malonate in positions

Table 1
Inhibition efficiencies of selected malonate-based compounds expressed as half maximal inhibitory concentration (IC_{50}).

Compound	Code	IC_{50} [μM]
Malonate	M1	67 ± 1
2-Hydroxymalonate	M2	94 ± 1
2-Aminomalonate	M3	400 ± 100
2,2-Dichloromalonate	M4	57 ± 1
2-Chloromalonate	M6	780 ± 100
2-Methylmalonate	M10	1850 ± 210
2,2-Difluoromalonate	M11	2160 ± 200
2,2-Dimethylmalonate	M16	5630 ± 510
2-Thiofenmalonate	M17	7030 ± 480
2,2-Bis(hydroxymethyl)malonate	M20	40,600 ± 11,000

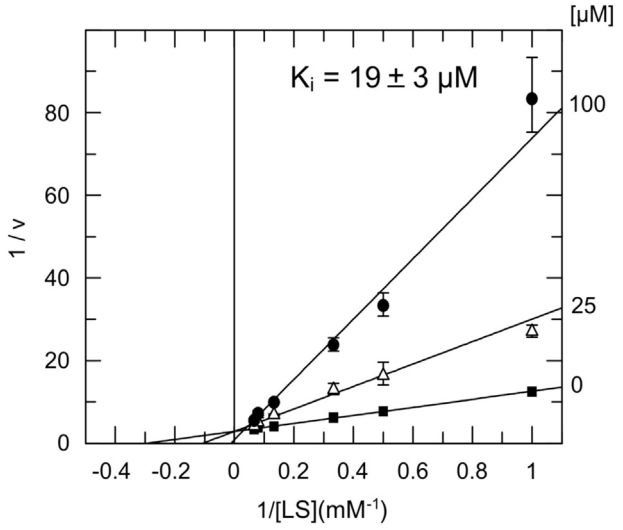

Fig. 2. Characterization of the most potent mSR inhibitor, 2,2-dichloromalonate. Double reciprocal Lineweaver–Burk plot showing the competitive mechanism of inhibition of mSR by 2,2-dichloromalonate. LS = L-serine. The data points are average of duplicates. K_i value was determined by non-linear regression fitting of initial reaction rates to the Michaelis–Menten equation. Data were processed in the program GraFit 5.0.4 [37].

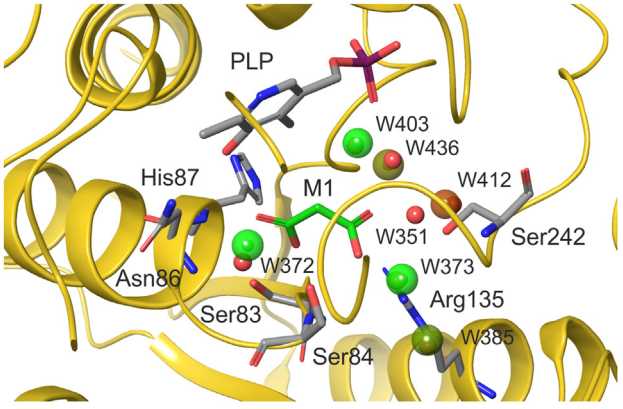

Fig. 3. The hSR/malonate X-ray structure (PDB code: 3L6B) [14] and active-site waters. WaterMap was used to infer positions of long-residence waters (larger spheres, coloured from brown – unfavourable free energy – to green – favourable free energy). Smaller red spheres show the X-ray water positions. Colour coding: yellow ribbon – hSR, light green sticks – carbon atoms of malonate, grey sticks – carbon atoms of hSR and PLP, red sticks – oxygens, blue sticks – nitrogens, purple sticks – phosphorus. Hydrogen atoms are not shown for the sake of clarity. The figure was prepared with Maestro [39].

Table 2
Direct and water (W) mediated hydrogen bond distances in the crystal structure of the hSR/malonate complex (PDB code 3L6B) [14] and in modelled complexes of hSR with redocked M1, M4, M16 and M20. The models were obtained by use of Glide docking using three waters as part of hSR followed by PM6-D3H4X/COSMO optimization. Heavy…heavy atom distances are shown with hydrogen…heavy atom distances indicated in parentheses. The distances are in Å.

Hydrogen bond distances					
	M1: X-ray	M1: redocked	M4	M16	M20
Main-chain					
Ser84:N	O9: 3.0	2.9 (2.0)	2.7 (1.9)	2.8 (2.0)	2.7 (1.8)
Asn86:N	O8: 3.3	3.4 (3.0)	3.2 (2.6)	3.2 (2.8)	3.3 (2.8)
His87:N	O8: 2.8	2.8 (1.8)	3.1 (2.1)	2.8 (1.8)	2.8 (1.8)
Side-chain					
Ser83:OG	O9: 2.6	2.6 (1.6)	2.6 (1.7)	2.6 (1.6)	2.6 (1.7)
Ser84:OG	O7: 2.6	2.6 (1.7)	2.6 (1.8)	2.6 (1.7)	2.6 (1.8)
Arg135:NH1	O7: 2.9	2.8 (1.7)	2.8 (1.8)	2.7 (1.7)	2.7 (1.7)
Arg135:NH2	O6: 3.0	3.2 (2.2)	3.0 (2.0)	3.2 (2.3)	2.9 (1.9)
Ser242:OG	O6: 3.1	2.8 (1.8)	2.7 (1.8)	2.7 (1.8)	2.7 (1.8)
Waters					
W351	O6: 3.0	–	–	–	–
W372	O8: 3.1	3.0 (2.2)	2.9 (2.1)	2.8 (1.9)	3.2 (2.5)
W373	O7: 2.8	2.7 (1.8)	2.8 (1.9)	2.7 (1.8)	2.7 (1.8)
W403	O6: 2.8	2.7 (1.8)	3.1 (2.1)	2.9 (2.0)	3.2 (2.3)
W436	O6: 3.4	–	–	–	–

similar to X-ray (Fig. 3) with a single exception: W351 was removed. (This finding confirmed the results of the X-ray structure analysis above and made us thus confident to remove W351 from the hSR/malonate model.) Five of these six water molecules identified by WaterMap made direct bridges between the protein and the ligand, three participate in water networks (Table 3). Five waters have occupancy close to 1.0 and one has occupancy of 0.8 (Table 3). The thermodynamic signatures can be seen in Table 3.

Three water molecules (W372, W373 and W403) have favourable free energy contributions. This is broken down into favourable enthalpy offset by unfavourable entropy. The other three waters (W385, W436 and W412) have unfavourable free energy. For W385 and W436 this is caused by a smaller favourable enthalpy as compared to the larger unfavourable entropy, whereas for W412 both enthalpy and entropy are unfavourable.

2.3.3. *Glide docking of malonate-based inhibitor series*

In order to predict the binding modes of malonate-based inhibitors we carried out standard docking, i.e. without any explicit water molecules. All of the compounds from Fig. 1 docked into malonate-like binding mode except M13. The reason was probably that a hydrophobic planar aromatic side chain could not fit into the tubular polar binding cavity because of the clashes with Ser84, Asn86, Lys114 and Gly239.

Having assessed the importance of three crystal water molecules (W372, W373 and W403) for the stability of the hSR/malonate complex (see above and Table 3), we carried out docking including these three water molecules as part of the protein. In this more realistic setup, the good binders M1–M11 retained the malonate-like binding mode (Fig. 4), while weakly binding compounds M12–M21 (except M16 and M20) did not dock into this solvated hSR active site. The weak binding of M16 and M20 is thus probably not determined by the binding mode but rather the energetics (see below).

2.3.4. *SQM optimizations of malonate-based inhibitors docked into hSR with three crystal waters*

For a detailed understanding of the differences in affinity, we undertook optimizations of the nine docked compounds with measured IC_{50} (*cf.* Table 1) on the semiempirical QM (SQM) level

Table 3
Thermodynamic signatures (ΔG_{solv}, ΔH_{solv} and $-T\Delta S_{solv}$, in kcal/mol) and average number of hydrogen bonds (#HB) of active-site waters in hSR/malonate X-ray complexes as determined by WaterMap. P, L and W stand for protein, ligand and water, respectively. Waters are sorted by ascending ΔG_{solv}.

	ΔG_{solv}	ΔH_{solv}	$-T\Delta S_{solv}$	#HB (PW)	#HB (LW)	#HB (WW)	Occupancy
W372	−3.7	−7.6	4.0	2.0	0.7	0.0	0.90
W403	−3.5	−9.4	5.9	1.7	1.0	0.0	1.00
W373	−3.0	−8.8	5.8	1.7	1.0	0.8	1.00
W385	1.4	−3.1	4.5	0.2	0.0	2.5	0.96
W436	2.4	−3.4	5.8	2.0	0.0	0.0	1.00
W412	4.6	1.7	2.9	0.7	0.3	0.6	0.78

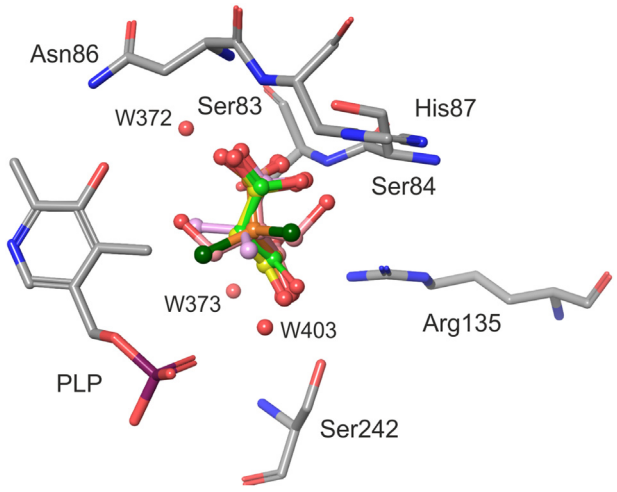

Fig. 4. Binding modes of selected malonate-based inhibitors (M1, M4, M16 and M20) in the hSR active site obtained by Glide docking with three crystal waters (W372, W373, W403) in place. Note that the view is rotated by ca. 90° compared to Fig. 3. Colour coding: carbon atoms of the inhibitors are represented by differently coloured sticks: light green – crystal M1, yellow – redocked M1, orange – M4, light purple – M16 and pink M20. hSR, PLP and waters are coloured as in Fig. 3. Hydrogen atoms are not shown for the sake of clarity. The figure was prepared with Maestro v. 9.9.

with corrections for close contacts (see Methods) coupled with the COSMO implicit solvent model [40]. This procedure retained the crystallographic malonate-like binding mode including the hydrogen-bonding interactions (Table 2).

SQM optimizations refined the hydrogen bonding interactions (Table 2) and did not change much the docked pose. For substitutions pointing toward W403, close contacts were sometimes observed. More complex rearrangements of water molecules as suggested by preliminary WaterMap predictions (not shown) might however be beyond the possibilities of gradient optimization.

Table 4
Experimental IC_{50} values for compounds from Table 1 and calculated SQM scores with their terms are shown. The SQM terms were calculated on the SQM optimized geometries of hSR/inhibitor complexes obtained from docking with three water molecules as part of protein.

Compound	IC_{50} (μM)	$RT^*\ln(IC_{50}/2)$	SQM score	ΔE_{int}	$\Delta\Delta G_{solv}$	$\Delta G'^{w}_{conf}$(L)	$-T\Delta S$ (L)
M1	67	−6.1	−106.2	−227.7	118.4	1.1	2.0
M2	94	−5.9	−106.3	−236.2	125.8	1.2	3.0
M3	400	−5.0	−115.2	−202.4	78.8	5.4	3.0
M4	57	−6.2	−97.0	−206.5	106.2	1.3	2.0
M6	780	−4.6	−101.2	−215.7	110.7	1.7	2.0
M10	1850	−4.1	−111.2	−233.5	118.2	1.1	3.0
M11	2160	−4.0	−93.8	−197.7	101.1	0.8	2.0
M16	5630	−3.5	−99.6	−233.0	128.0	1.4	4.0
M20	40,600	−2.3	−97.5	−255.1	141.4	10.2	6.0

2.3.5. SQM scoring and terms

Table 4 shows SQM score and terms and their comparison with the experimental IC_{50} values. It can be seen that with the exception of M4 the scores for compounds M1–M10 are larger than −101 kcal/mol, while those for compounds M11–M20 are lower. This separates the inhibitors with affinities higher and lower than 2 mM. Additionally, the score of compound M3 is overestimated. It has a different charge (−1) than the other inhibitors (−2) due to its NH_3^+ group. Our corrected SQM method provides reliable estimates of gas-phase binding energy with errors within few kcal/mol [41]. The treatment of solvation free energy is, however, compromised by much bigger errors [42], which is especially true when solvation free energies of complexes with different charge (which is the present case) are compared. The most effective inhibitor M4 can be underestimated due to the close contacts with W403. The description of possible rearrangements of waters would require dynamic treatment and is beyond the scope of this article.

Closer inspection of the individual terms revealed a large overestimation of values of the vacuum interaction (ΔE_{int}) with the values around −200 kcal/mol. These values caused by multiple charged interactions were offset by $\Delta\Delta G_{solv}$ on the order of 100 kcal/mol. A small note is that the weakest ligand, M20, has prominent penalties for ligand deformation and entropy. Note that the overall score for all the compounds is too large due to the neglect of terms such as e.g. protein deformation or vibrational entropy. These are not included here due to their computational demands.

3. Discussion

Due to its role in biosynthesis of the neurotransmitter D-serine, serine racemase has become a promising target for pharmaceutical intervention in neurological diseases caused by overstimulation of NMDARs. Nevertheless, no highly potent inhibitor of this enzyme has been identified to date. Malonate, one of the most potent inhibitors described, still possesses a high inhibition constant of 71 ± 16 μM [17]. More potent specific SR inhibitors are thus desirable. In this study, we investigated whether α-carbon modifications of malonate could lead to an increase in inhibitory potency. We screened 20 malonate-based compounds for inhibition of mSR.

Our results suggest that malonate derivatives with small polar groups on the α-carbon (be it mono- or di-substitution, M1–M9) possess higher binding affinities than compounds with hydrophobic and bulky moieties (M12–M21). However, the efficiency with which a particular compound inhibits mSR does not correlate in a straightforward manner with its polarity or the size of the α-carbon substituent.

Further characterization of selected inhibitors revealed that 2,2-dichloromalonate is the only compound from the panel with higher affinity towards SR than malonate itself (K_i = 19 ± 3 μM). It should be noted that the K_i value for malonate determined in this study was 3-fold lower than the value previously published by our research group [17]. This difference was likely caused by slightly different preparation of the recombinant enzyme. Very recently, Mori et al. published a series of novel inhibitors of human serine racemase designed by *in silico* virtual screening [21]. It is difficult to compare their binding with our data directly since the authors did not determine the mechanism of action of their inhibitors and could thus not provide the K_i values of their compounds. Since they used different reaction conditions, the IC_{50} data that they report are not directly comparable. The computational approach of Mori et al.

entailed pharmacophoric similarity searches, Glide docking and scoring excluding water molecules and cluster 2D fingerprint analysis. This procedure offered much larger inhibitor than malonate due to the possibility of occupying the water-filled tunnel leading to Ile236. The missing theoretical treatment of water thermodynamics was replaced by experimental testing.

To understand the binding affinities of the compound series, we used the available 3D structure of the hSR/malonate complex [14] and performed a computational analysis of the active-site hydration using WaterMap, followed by Glide docking [43] and semi-empirical quantum mechanics-based scoring [44]. Although the inhibitory activities of the compounds were determined by competitive assay using recombinant mSR, computational rationalization using the structure of the human orthologue of the enzyme was possible. Indeed, it has been shown that kinetic data obtained using recombinant mSR are very similar to those obtained with hSR [45]. Moreover, the residues forming the active site of hSR (within a distance of 4 Å from active-site-bound malonate) are conserved on the sequence level in mSR (S83-S84-G85-N86-H87, R136, N156, G243 and S246).

The active site of hSR is highly polar, open to the bulk solvent and filled with several structural water molecules, even in the presence of the malonate inhibitor. Structural water molecules are usually retained in calculations, as they are known to play important roles in determining structures and energetics of protein–ligand complexes [46]. Indeed, as shown previously, they can bring tens of kcal/mol to the binding energetics. The X-ray structure contained a problematic water molecule W351 which had a repulsive contact of 2.27 Å with W436 and Ser242 and its ADP (atomic displacement parameter, formerly B-factor) was too high. We propose that this problem in the crystallographic model could be overcome by an alternative crystallographic refinement of W351 that would lead to lower occupancy and ADP. To assess the hydration structure of hSR/malonate complex, we have performed a WaterMap calculation which showed that W351 should be removed from the model. We thus consider hydration analysis of the active-site (using WaterMap [25] or related tools, such as GRID [22], JAWS [23] or HINT [24]) a crucial step in discussing any structure–activity relationship in hSR.

The Cα substituents of the malonate analogues may cause fewer water molecules to fit in the hSR active site. Indeed, for M4 and M16, the presence of W403 creates repulsive close contacts which are only partially relieved by our SQM optimizations. However, this water molecule (and maybe also the adjacent water network) would likely rearrange or even be expelled, which would deserve a future detailed analysis.

The extremely high surface charge density of malonate and its analogues presents a challenge for computations. The gas-phase interaction energies were large due to the polar and charged interactions. These interactions were damped by the solvent, giving rise to the overall energetics. However, some computationally demanding scoring terms (protein deformation, entropy) were not treated and thus the binding free energies were too negative in comparison with the experiment.

The SQM scores with the most stable variants of each compound resulted in a rough estimate of the stronger vs. weaker binders (the borderline was IC_{50} of 2 mM and SQM score of −101 kcal/mol). However, a detailed dynamical treatment of the active-site hydration proved critical for interpreting the experimental results. The results suggest that binding of the strongest inhibitor M4 is underestimated because a limited description of the rearrangement or even expulsion of one water molecule (W403).

4. Conclusions

In this work, we tested a series of malonate-based compounds as potential inhibitors of mSR and identified 2,2-dichloromalonate as the most effective competitive inhibitor known to date.

Using the published crystal structure of the hSR/malonate complex, we performed a computational analysis of active-site hydration, binding mode and affinities, which allowed us to distinguish between stronger and weaker binding compounds. The inhibitor-bound active site of hSR is filled with structural water molecules, the occupancies of which are sometimes doubtful and must be assessed with computational tools. The theoretical issues raised here can aid further progress in the computational search for more effective SR inhibitors, which would alleviate the necessity to experimentally test large numbers of compounds. Novel potent hSR inhibitors may then become leads for development of new strategies to treat diseases caused by NMDAR overactivation.

5. Materials and methods

5.1. Materials

Compounds M1, M9, M10, M15, M16, M17 and M19 (Fig. 1) were purchased from Sigma–Aldrich; compound M2 was purchased from Alfa Aesar. Reagents and solvents for preparation of compound M11 were purchased from Alfa Aesar; reagents and solvents for preparation of the remaining compounds were purchased from Sigma–Aldrich.

Mass spectra were measured on an LCQ Fleet spectrometer (Thermo Fisher Scientific) using ESI ionization. High-resolution mass spectra were measured on an LTQ Orbitrap XL spectrometer (Thermo Fisher Scientific) using ESI ionization. The ^{13}C and ^{19}F NMR spectra were obtained on a Varian UNITYINOVA-300 spectrometer.

Enzymatic reaction mixtures were analyzed using a Zorbax Extend C18 reversed phase HPLC column (4.6 × 250 mm, particle size 5 μm, Agilent Technologies, USA) mounted on an Alliance 2795 HPLC system (Waters Co., Milford, MA, USA) coupled to a Waters 2487 dual wavelength absorbance detector.

5.2. Preparation of malonate-based compounds

Compound M11 (Fig. 1) was prepared by alkaline hydrolysis of diethyl difluoromalonate, as previously described [47]. The compound was analyzed using ^{13}C and ^{19}F NMR spectrometry, the spectral data have already been published [47]. The purity of the compound was higher than 95%.

Compounds M3–M8, M12–M14, M18, M20 and M21 (Fig. 1) were prepared by non-aqueous saponification. The starting malonic acid diesters (5 mmol) were added into a solution of 440 mg (11 mmol) of NaOH in 150 ml of 99% ethanol (1.1 equivalents for each ester group). This mixture was heated at 80 °C for 2 h, resulting in quantitative precipitation of corresponding disodium salts. The mixture was subsequently heated under reflux for 5 min and then cooled to 0 °C. This heating and cooling was repeated twice to get a well-filterable solid product. The solid product was filtered off, washed with 99% ethanol (2 × 30 ml) and dried under high vacuum (0.01 mbar) at 60 °C for 2 days. For the identity and purity analysis see the supporting information. The purity of the tested compounds was determined by the combustion analysis (C, H, N) and was higher than 95%.

5.3. mSR expression and purification

Mouse SR was prepared as described [17] with some modifications. Briefly, the plasmid pKS-mSR was transformed into calcium

chloride competent *E. coli* MC1061. Bacteria were cultivated in growth medium containing ampicillin at 37 °C and 300 rpm to $OD_{595} = 0.9$. Production of mSR was induced with 1 mM L-arabinose. Five hours after induction, cell cultures were harvested by centrifugation (10,000 *g*, 10 min, 4 °C), and bacteria were lysed in QA buffer (20 mM triethanolamine hydrochloride-NaOH, pH 7.4, 1 mM $MgCl_2$, 20 μM pyridoxal 5′-phosphate, 100 μM DL-dithiothreitol, and 0.02% (w/v) NaN_3) containing 200 μg/ml chicken egg lysozyme, complete EDTA-free protease inhibitor mix (Roche Molecular Biochemicals), 0.05% (w/v) sodium deoxycholate and 10 μg/ml DNaseI. Mouse SR was purified using a four-step procedure: ammonium sulphate precipitation, reverse phase chromatography (Phenyl-Sepharose FastFlow, Pharmacia), ion-exchange chromatography (Q-Sepharose, FastFlow, Pharmacia), and affinity chromatography (ATP-agarose, Sigma). Collected fractions from affinity chromatography were dialyzed against 500 volumes of QA buffer at 4 °C. The mSR solution was concentrated to 23.6 mg/ml and stored at −70 °C.

5.4. Activity assays

Enzymatic activities of mSR were determined as previously described [17]. Briefly, activity reactions were carried out at 37 °C in a pH 8.0 buffer containing 100 mM HEPES-NaOH, 10 μM pyridoxal 5′-phosphate, 1 mM $MgCl_2$, 5 mM DL-dithiothreitol, and 1 mM ATP. The mSR concentration was kept at 10 μg/ml (~135 nM) while the concentrations of L-serine and test compounds depended on the experiment type. In the initial screening, the concentrations of both L-serine and test compound were equal (5 mM). To determine IC_{50} values, 10 different inhibitor concentrations were used, while the concentration of L-serine remained constant at 5 mM. The inhibitor concentrations were chosen based on the initial screening results. In experiments aiming to determine the mechanism of inhibition, different concentrations of L-serine (ranging from 1 mM to 15 mM) and inhibitor (ranging from 0 mM to 150 mM) were used. Reactions were performed in duplicate in a final volume of 100 μl and stopped by addition of $HClO_4$ after 20–25 min. The resulting solutions were neutralized with KOH. Glycine was added as an internal standard. The reaction mixtures were derivatized with Marfey's reagent and analyzed by reversed-phase HPLC.

5.5. Structure preparation

The starting geometry was taken from the X-ray structure of the hSR/malonate complex (PDB code 3L6B) [14]. For docking by use of Glide software, Schrodinger [43] the structure was processed with the Schrödinger Suite 2014-3 Protein Preparation Wizard tool [48]. This tool automatically set charge (+2) and a correct atom type to the Mn^{2+} atom and the orientation of any flipped side chains of Asn, Gln amide groups or His imidazole groups. For the PLP cofactor, bond orders and formal charges (total charge of −2) were set automatically and the structure was manually modelled in a ketoamine tautomer as a Schiff base internal aldimine with Lys56. In place of the missing loop between residues 68 and 74 of hSR, the flanking C- and N-residues were capped by N-methyl amide and acetyl moieties, respectively. In cases of alternate side chain conformation (Gln89, Cys269), the A conformation was used. The charge states of the amino acid side chains and the N- and C-termini were assigned to match the experimental pH of 8.0 ± 0.5 using Epik v2.9 of Schrodinger Suite 2014-3 [48]. For Glide docking and SQM calculations, all the crystallographic water molecules were removed at the onset. Based on the results of WaterMap analysis (see Results) waters W372, W373, and W403 were included. For WaterMap calculations all the crystal waters were used. An exhaustive sampling of the orientations of groups whose hydrogen bonding network needed to be optimized, was performed. Finally, the protein structure was refined to relieve of steric clashes by use of a restrained minimization with the OPLS2005 force field [49] until a final RMSD of 0.03 Å with respect to the input protein coordinates was achieved.

5.5.1. Glide docking

The malonate-based compounds were built using Maestro 9.9.013 [39] or converted from 2D to 3D structures using LigPrep version 3.1.013 [50]. The protein structure, prepared as described above, was used to build the energy grid. A van der Waals radius scaling factor of 0.5 for atoms with a partial atomic charge (absolute value) less than 0.15 was used in order to soften the potential for nonpolar parts of the receptor. The enclosing box was centred on the malonate residue, and default sizes were used for both the enclosing and bounding box. The malonate-based inhibitors were docked into hSR by use of Glide v6.4.013 [43]. The SP docking protocol was used. Ligands were docked flexibly, the sampling of ring conformations was included, and nonplanar amide conformations were penalized. SP docking was performed selecting 100 poses per ligand to be energy minimized on the OPLS-AA nonbonded-interaction grid (see above). All other parameters were set to their default values. Docking results poses with high Glide score and Glide Emodel energy conformations and malonate-like binding mode geometries were considered.

5.5.2. WaterMap calculations

WaterMap is a molecular dynamics-based method that predicts the locations, enthalpy (ΔH_{solv}) and entropy ($-T\Delta S_{solv}$) of water molecules in the solvation layer of proteins or protein–ligand complexes, where ΔH_{solv} and $T\Delta S_{solv}$ are the enthalpy and entropy of each water molecule relative to that in bulk medium. The theoretical basis and computational algorithms of WaterMap are described elsewhere [51,52]. Standard settings were used for the WaterMap 2.0013 calculations, except the removal of all residues outside a 10 Å shell around the inhibitor, i.e. the whole protein–ligand complex was used. The non-hydrogen atoms of the protein residues (and inhibitor where applicable) were restrained using a 5 kcal mol^{-1} $Å^{-1}$ force constant. The protein and added solvent were then relaxed during 4000 cycles of energy minimisation until reaching convergence at a final 5 kcal mol^{-1} $Å^{-1}$ gradient. Three short molecular dynamics (MD) simulations followed the minimisation. The first 12 ps of MD are run at constant volume and temperature (NVT, 10 K) followed by a second 12 ps MD simulation at a constant temperature of 10 K and constant pressure at 1 atm (NPT). The system was then equilibrated during 120 ps of MD simulation at a constant temperature of 300 K and 1 atm pressure (NPT). After equilibration, a production molecular dynamics (MD) run of 2.0 ns was performed under NPT conditions at 300 K and 1 atm pressure, saving frames every 1.5 ps. WaterMap was run from Maestro using all the crystallographic waters. The analysis of the resulting MD frames with inhomogenous fluid theory (IFT) [53] using WaterMap yielded the clustered water positions for hydration sites with high occupancy and their average enthalpy, entropy and free energy deviations from those of bulk solvent. Our analysis focused on six crystallographic water molecules within two solvation layers (i.e. 4.4 Å) of the malonate (W372, W373, W385, W403, W412 and W436). Running in parallel on 2 processors on a Linux system the entire procedure was usually completed within 48 h. Visualisation was done with Maestro v 9.9.013 [39].

5.6. Semiempirical quantum mechanics (SQM) optimizations

For SQM calculations, the structural open-shell Mn^{2+} cation was replaced with closed-shell Mg^{2+}. The complexes were subjected to

SQM optimizations using the linear-scaling PM6-D3H4X method MOZYME available in MOPAC2009. To increase efficiency, only protein residues within a distance of 8 Å from the inhibitors were considered (about 1100 atoms) in optimization and combined with a homogenous COSMO solvent [40]. To simulate the structural constraints of the protein frame, only residues within a distance of 6 Å from the inhibitor were optimized, while the rest were kept frozen. Similar sizes of QM regions in another protein–ligand system have previously been shown to be optimal [35]. The PM6-D3H4X method reliably describes various types of noncovalent interactions such as dispersion, hydrogen- and halogen-bonding [41,54].

5.7. SQM score and its terms

The interaction energies were calculated at the PM6-D3H4X/COSMO level for the whole hSR/inhibitor complexes optimized using the procedure described above. The interaction energies were obtained as the difference between the energy of the complex and the energies of the ligands and the enzyme with the three waters. The PM6-D3H4X/COSMO energies were split into their vacuum and solvation contributions.

The SQM scores were calculated according to Eq. (1) [28].

$$\text{Score} = \Delta E_{\text{int}} + \Delta\Delta G_{\text{solv}} + \Delta G'^{\,\text{w}}_{\text{conf}}(\text{L}) - T\Delta S_{\text{rot}} \quad (1)$$

where

$$\Delta\Delta G_{\text{solv}} = \Delta\Delta G_{\text{int,solv}} + \left(\Delta G^{\text{low}}_{\text{solv}}(\text{L}) - \Delta G^{\text{high}}_{\text{solv}}(\text{L})\right) \quad (2a)$$

$$\Delta G'^{\,\text{w}}_{\text{conf}}(\text{L}) = \Delta E_{\text{def}}(\text{L}) + \Delta\Delta G_{\text{conf,solv}}(\text{L}) \quad (2b)$$

Particular terms describe the gas-phase interaction energy (ΔE_{int}), the interaction solvation/desolvation free energy ($\Delta\Delta G_{\text{solv}}$; Eq. (2a)), the change of the conformational free energy of the ligand ($\Delta G'^{\,\text{w}}_{\text{conf}}(\text{L})$; Eq. (2b)), and the entropy change upon binding ($T\Delta S_{\text{rot}}$).

For the solvation free energy (Eq. (2a)), COSMO is used as the "low" method, whereas SMD is used as the "high" method, due to its superior performance for charged ligands [44]. The $-T\Delta S_{\text{rot}}$ is evaluated as the number of ligand rotatable bonds which become hindered upon complexation – the penalty is 1 kcal.mol^{-1} for each.

5.8. Correction for close contacts in PM6-D3H4X

Repulsion between two noncovalently bound atoms is underestimated in the PM6-D3H4X method (similar to other SQM methods) due to the use of core–core repulsion instead of exact atom–atom repulsion. Because the docking procedure yields structures with very close hydrogen–hydrogen contacts, we had to slightly modify our corrections for the PM6 method. We had already found that PM6 itself underestimates the repulsion between hydrogen atoms and we added a correction for this to the D3 dispersion correction [41]. This correction consists of sigmoidal repulsive potential applied to each pair of hydrogens (equation (11) in the original paper). It was parameterized on CCSD(T)/CBS hydrocarbon dissociation curves starting at 80% of the equilibrium distance from the S66x8 data set [55]. Later, we found that this correction is not strong enough to correct the error of PM6 at even shorter distances, such as the ones produced by docking where close contacts as short as 60% of the equilibrium distance occur. Therefore, we developed a new correction that acts even at these distances. Reparametrization of the original potential was not sufficient and it was replaced by an exponential of the form:

$$E_{\text{rep}}(r) = k^{*}\exp(-a^{*}r^{b}) \quad (3)$$

where k, a and b are the parameters. To damp the correction at covalent distances, we define two cutoff radii, $r_0 = 1.0$ Å and $r_1 = 1.5$ Å. At distances $r > r_1$, equation (3) is used as it is. For $r < r_0$, the correction has a constant value of $E_{\text{rep}}(r_0)$. In the intermediate region, the value of the potential is calculated using a polynomial constructed to provide a smooth transition between these segments. The polynomial is not given explicitly but constructed on the fly so that its values and first and second derivatives at r_0 and r_1 equal to the ones of the adjacent segments of the curve.

The parameters were optimized on a dissociation curve of a methane dimer in a geometry where the two hydrogens point against each other. The curve starts at hydrogen–hydrogen distance of 1.6 Å, the energies were calculated using the same CCSD(T)/CBS as used in the S66x8 data set [55]. The resulting parameters are $k = 117.726$, $a = 1.540$ and $b = 1.729$ in the Å/kcal mol^{-1} unit system. The new repulsion correction improves the behaviour of PM6-D3H4 at the shortest distances, eliminating the false minima found in the structures obtained from docking. At distances above 80% of the equilibrium, it closely mimics the original PM6-D3H4 results.

Acknowledgements

We would like to thank Jiří Schimer for synthesis of 2,2-difluoromalonate, Rüdiger Ettrich for help with protein modelling and Hillary Hoffman for language corrections. This work was part of Research Project RVO 61388963 awarded by the Academy of Sciences of the Czech Republic. We acknowledge the financial support of the Czech Science Foundation [P208/12/G016] and the operational program Research and Development for Innovations of the European Social Fund (CZ 1.05/2.1.00/03/0058). We also thank Gilead Sciences and IOCB Research Centre for financial support.

Appendix A. Supplementary data

Supplementary data related to this article can be found at http://dx.doi.org/10.1016/j.ejmech.2014.10.043.

References

[1] L.V. Kalia, S.K. Kalia, M.W. Salter, NMDA receptors in clinical neurology: excitatory times ahead, Lancet Neurol. 7 (2008) 742–755.
[2] R. Dingledine, K. Borges, D. Bowie, S.F. Traynelis, The glutamate receptor ion channels, Pharmacol. Rev. 51 (1999) 7–61.
[3] W. Danysz, C.G. Parsons, Glycine and N-methyl-D-aspartate receptors: physiological significance and possible therapeutic applications, Pharmacol. Rev. 50 (1998) 597–664.
[4] S.A. Fuchs, R. Berger, T.J. de Koning, D-serine: the right or wrong isoform? Brain Res. 1401 (2011) 104–117.
[5] P. Conti, L. Tamborini, A. Pinto, A. Blondel, P. Minoprio, A. Mozzarelli, C. De Micheli, Drug discovery targeting amino acid racemases, Chem. Rev. 111 (2011) 6919–6946.
[6] B. Campanini, F. Spyrakis, A. Peracchi, A. Mozzarelli, Serine racemase: a key player in neuron activity and in neuropathologies, Front. Biosci. (Landmark Ed.) 18 (2013) 1112–1128.
[7] N. Canu, M.T. Ciotti, L. Pollegioni, Serine racemase: a key player in apoptosis and necrosis, Front. Synaptic Neurosci. 6 (2014) 9.
[8] H. Wolosker, S. Blackshaw, S.H. Snyder, Serine racemase: a glial enzyme synthesizing D-serine to regulate glutamate-N-methyl-D-aspartate neurotransmission, Proc. Natl. Acad. Sci. U. S. A. 96 (1999) 13409–13414.
[9] S.P. Cook, I. Galve-Roperh, A. Martinez del Pozo, I. Rodriguez-Crespo, Direct calcium binding results in activation of brain serine racemase, J. Biol. Chem. 277 (2002) 27782–27792.
[10] K. Strisovsky, J. Jiraskova, C. Barinka, P. Majer, C. Rojas, B.S. Slusher, J. Konvalinka, Mouse brain serine racemase catalyzes specific elimination of L-serine to pyruvate, FEBS Lett. 535 (2003) 44–48.
[11] A. Neidle, D.S. Dunlop, Allosteric regulation of mouse brain serine racemase, Neurochem. Res. 27 (2002) 1719–1724.

[12] D.S. Dunlop, A. Neidle, Regulation of serine racemase activity by amino acids, Brain Res. Mol. Brain Res. 133 (2005) 208–214.
[13] J. Jiraskova-Vanickova, R. Ettrich, B. Vorlova, H.E. Hoffman, M. Lepsik, P. Jansa, J. Konvalinka, Inhibition of human serine racemase, an emerging target for medicinal chemistry, Curr. Drug Targets 12 (2011) 1037–1055.
[14] M.A. Smith, V. Mack, A. Ebneth, I. Moraes, B. Felicetti, M. Wood, D. Schonfeld, O. Mather, A. Cesura, J. Barker, The structure of mammalian serine racemase: evidence for conformational changes upon inhibitor binding, J. Biol. Chem. 285 (2010) 12873–12881.
[15] H. Wolosker, Serine racemase and the serine shuttle between neurons and astrocytes, Biochim. Biophys. Acta 1814 (2011) 1558–1566.
[16] M. Marchetti, S. Bruno, B. Campanini, A. Peracchi, N. Mai, A. Mozzarelli, ATP binding to human serine racemase is cooperative and modulated by glycine, FEBS J. 280 (2013) 5853–5863.
[17] K. Strisovsky, J. Jiraskova, A. Mikulova, L. Rulisek, J. Konvalinka, Dual substrate and reaction specificity in mouse serine racemase: identification of high-affinity dicarboxylate substrate and inhibitors and analysis of the beta-eliminase activity, Biochemistry 44 (2005) 13091–13100.
[18] H.E. Hoffman, J. Jiraskova, P. Cigler, M. Sanda, J. Schraml, J. Konvalinka, Hydroxamic acids as a novel family of serine racemase inhibitors: mechanistic analysis reveals different modes of interaction with the pyridoxal-5'-phosphate cofactor, J. Med. Chem. 52 (2009) 6032–6041.
[19] R. Panizzutti, J. De Miranda, C.S. Ribeiro, S. Engelender, H. Wolosker, A new strategy to decrease N-methyl-D-aspartate (NMDA) receptor coactivation: inhibition of D-serine synthesis by converting serine racemase into an eliminase, Proc. Natl. Acad. Sci. U. S. A. 98 (2001) 5294–5299.
[20] S. Dixon, K.M. Merz Jr., G. Lauri, J.C. Ianni, QMQSAR: utilization of a semi-empirical probe potential in a field-based QSAR method, J. Comput. Chem. 26 (2005) 23–34.
[21] H. Mori, R. Wada, J. Li, T. Ishimoto, M. Mizuguchi, T. Obita, H. Gouda, S. Hirono, N. Toyooka, In silico and pharmacological screenings identify novel serine racemase inhibitors, Bioorg. Med. Chem. Lett. 24 (2014) 3732–3735.
[22] P.J. Goodford, A computational procedure for determining energetically favorable binding sites on biologically important macromolecules, J. Med. Chem. 28 (1985) 849–857.
[23] A. Amadasi, J.A. Surface, F. Spyrakis, P. Cozzini, A. Mozzarelli, G.E. Kellogg, Robust classification of "relevant" water molecules in putative protein binding sites, J. Med. Chem. 51 (2008) 1063–1067.
[24] J. Michel, J. Tirado-Rives, W.L. Jorgensen, Energetics of displacing water molecules from protein binding sites: consequences for ligand optimization, J. Am. Chem. Soc. 131 (2009) 15403–15411.
[25] R. Abel, T. Young, R. Farid, B.J. Berne, R.A. Friesner, Role of the active-site solvent in the thermodynamics of factor Xa ligand binding, J. Am. Chem. Soc. 130 (2008) 2817–2831.
[26] K. Raha, M.B. Peters, B. Wang, N. Yu, A.M. Wollacott, L.M. Westerhoff, K.M. Merz Jr., The role of quantum mechanics in structure-based drug design, Drug Discov. Today 12 (2007) 725–731.
[27] R.A. Bryce, Physics-based scoring of protein-ligand interactions: explicit polarizability, quantum mechanics and free energies, Future Med. Chem. 3 (2011) 683–698.
[28] M. Lepsik, J. Rezac, J. Kolar, A. Pecina, P. Hobza, J. Fanfrlik, The semiempirical quantum mechanical scoring function for in-silico drug design, ChemPlusChem 78 (2013) 921–931.
[29] K. Raha, K.M. Merz Jr., A quantum mechanics-based scoring function: study of zinc ion-mediated ligand binding, J. Am. Chem. Soc. 126 (2004) 1020–1021.
[30] A. Ciancetta, S. Genheden, U. Ryde, A QM/MM study of the binding of RAPTA ligands to cathepsin B, J. Comput. Aid. Mol. Des. 25 (2011) 729–742.
[31] J. Fanfrlik, J. Brynda, J. Rezac, P. Hobza, M. Lepsik, Interpretation of protein/ligand crystal structure using QM/MM calculations: case of HIV-1 protease/metallacarborane complex, J. Phys. Chem. B 112 (2008) 15094–15102.
[32] A. Pecina, M. Lepsik, J. Rezac, J. Brynda, P. Mader, P. Rezacova, P. Hobza, J. Fanfrlik, QM/MM calculations reveal the different nature of the interaction of two carborane-based sulfamide inhibitors of human carbonic anhydrase II, J. Phys. Chem. B 117 (2013) 16096–16104.
[33] P. Dobes, J. Rezac, J. Fanfrlik, M. Otyepka, P. Hobza, Semiempirical quantum mechanical method PM6-DH2X describes the geometry and energetics of CK2-inhibitor complexes involving halogen bonds well, while the empirical potential fails, J. Phys. Chem. B 115 (2011) 8581–8589.
[34] J. Fanfrlik, M. Kolar, M. Kamlar, D. Hurny, F.X. Ruiz, A. Cousido-Siah, A. Mitschler, J. Rezac, E. Munusamy, M. Lepsik, P. Matejicek, J. Vesely, A. Podjarny, P. Hobza, Modulation of aldose reductase inhibition by halogen bond tuning, ACS Chem. Biol. 8 (2013) 2484–2492.
[35] A. Pecina, O. Prenosil, J. Fanfrlik, J. Rezac, J. Granatier, P. Hobza, M. Lepsik, On the reliability of the corrected semiempirical quantum chemical method (PM6-DH2) for assigning the protonation states in HIV-1 protease/inhibitor complexes, Collect. Czech Chem. Commun. 76 (2011) 457–479.
[36] J. Fanfrlik, P.S. Brahmkshatriya, J. Rezac, A. Jilkova, M. Horn, M. Mares, P. Hobza, M. Lepsik, Quantum mechanics-based scoring rationalizes the irreversible inactivation of parasitic Schistosoma mansoni cysteine peptidase by vinyl sulfone inhibitors, J. Phys. Chem. B 117 (2013) 14973–14982.
[37] R.J. Leatherbarrow, GraFit Version 7, Erithacus Software Ltd., Horley, UK, 2009.
[38] Schrödinger Release 2014-3: WaterMap, Version 1.9, Schrödinger, LLC, New York, NY, 2014.
[39] Schrödinger Release 2014-3: Maestro, Version 9.9, Schrödinger, LLC, New York, NY, 2014.
[40] A. Klamt, G. Schuurmann, COSMO – a new approach to dielectric screening in solvents with explicit expression for the screening energy and its gradient, J. Chem. Soc. Perkin Trans. 2 (1993) 799.
[41] J. Rezac, P. Hobza, Advanced corrections of hydrogen bonding and dispersion for semiempirical quantum mechanical methods, J. Chem. Theory Comput. 8 (2012) 141–151.
[42] A.V. Marenich, C.J. Cramer, D.G. Truhlar, Universal solvation model based on solute electron density and on a continuum model of the solvent defined by the bulk dielectric constant and atomic surface tension, J. Phys. Chem. B 113 (2009) 6378–6396.
[43] Small-molecule Drug Discovery Suite 2014-3: Glide, Version 6.4, Schrödinger, LLC, New York, NY, 2014.
[44] J. Fanfrlik, A.K. Bronowska, J. Rezac, O. Prenosil, J. Konvalinka, P. Hobza, A reliable docking/scoring scheme based on the semiempirical quantum mechanical PM6-DH2 method accurately covering dispersion and H-bonding: HIV-1 protease with 22 ligands, J. Phys. Chem. B 114 (2010) 12666–12678.
[45] H.E. Hoffman, J. Jiraskova, M. Ingr, M. Zvelebil, J. Konvalinka, Recombinant Human Serine Racemase: Enzymologic Characterization and Comparison with its Mouse Ortholog, Protein Expr. Purif. 63 (2009) 62–67.
[46] S. Genheden, P. Mikulskis, L. Hu, J. Kongsted, P. Soderhjelm, U. Ryde, Accurate predictions of nonpolar solvation free energies require explicit consideration of binding-site hydration, J. Am. Chem. Soc. 133 (2011) 13081–13092.
[47] C.P. Horwitz, A. Ghosh, Synthesis of Macrocyclic Tetraamido Compounds and New Metal Insertion Process. Patent No. 7060818.
[48] Schrödinger Release 2014-3: Schrödinger Suite 2014-3 Protein Preparation Wizard, Schrödinger, LLC, New York, NY, 2014.
[49] J.L. Banks, H.S. Beard, Y. Cao, A.E. Cho, W. Damm, R. Farid, A.K. Felts, T.A. Halgren, D.T. Mainz, J.R. Maple, R. Murphy, D.M. Philipp, M.P. Repasky, L.Y. Zhang, B.J. Berne, R.A. Friesner, E. Gallicchio, R.M. Levy, Integrated modeling program, applied chemical theory (IMPACT), J. Comput. Chem. 26 (2005) 1752–1780.
[50] Schrödinger Release 2014-3: LigPrep, Version 3.1, Schrödinger, LLC, New York, NY, 2014.
[51] T. Young, R. Abel, B. Kim, B.J. Berne, R.A. Friesner, Motifs for molecular recognition exploiting hydrophobic enclosure in protein-ligand binding, Proc. Natl. Acad. Sci. U. S. A. 104 (2007) 808–813.
[52] K.J. Bowers, E. Chow, H. Xu, R.O. Dror, M.P. Eastwood, B.A. Gregersen, J.L. Klepeis, I. Kolossvary, M.A. Moraes, F.D. Sacerdoti, J.K. Salmon, Y. Shan, D.E. Shaw, Scalable algorithms for molecular dynamics simulations on commodity clusters, in: Proceedings of the ACM/IEEE Conference on Supercomputing (SC06), Tampa, Florida, November 11–17, 2006.
[53] Z. Li, T. Lazaridis, Thermodynamic contributions of the ordered water molecule in HIV-1 protease, J. Am. Chem. Soc. 125 (2003) 6636–6637.
[54] J. Rezac, P. Hobza, A halogen-bonding correction for the semiempirical PM6 method, Chem. Phys. Lett. 506 (2011) 286–289.
[55] J. Rezac, K.E. Riley, P. Hobza, S66: a well-balanced database of benchmark interaction energies relevant to biomolecular structures, J. Chem. Theory Comput. 7 (2011) 2427–2438.